NANO LETTERS

LETTER

pubs.acs.org/NanoLett

Porous One-Dimensional Nanostructures through Confined Cooperative Self-Assembly

Feng Bai,[†,‡] Zaicheng Sun,[‡,§] Huimeng Wu,[∥] Raid E. Haddad,[‡] Eric N. Coker,[∥] Jian Yu Huang,[∥] Mark A. Rodriguez,[∥] and Hongyou Fan*[,‡,∥]

[†]Key Laboratory for Special Functional Materials of the Ministry of Education, Henan University, Kaifeng 475004, People's Republic of China

[‡]Department of Chemical and Nuclear Engineering, The University of New Mexico/NSF Center for Micro-Engineered Materials, Albuquerque, New Mexico 87131, United States

[§]State Key Laboratory of Luminescence and Applications, Changchun Institute of Optics, Fine Mechanics, and Physics, Chinese Academy of Sciences, 3888 East Nanhu Road, Changchun 130033, People's Republic of China

[∥]Advanced Materials Laboratory, Sandia National Laboratories, 1001 University Boulevard SE, Albuquerque, New Mexico 87106, United States

Supporting Information

ABSTRACT: We report a simple confined self-assembly process to synthesize nanoporous one-dimensional photoactive nanostructures. Through surfactant-assisted cooperative interactions (e.g., $\pi-\pi$ stacking, ligand coordination, and so forth) of the macrocyclic building block, zinc meso-tetra (4-pyridyl) porphyrin (ZnTPyP), self-assembled ZnTPyP nanowires and nanorods with controlled diameters and aspect ratios are prepared. Electron microscopy characterization in combination with X-ray diffraction and gas sorption experiments indicate that these materials exhibit stable single-crystalline and high surface area nanoporous frameworks with well-defined external morphology. Optical characterizations using UV−vis spectroscopy and fluorescence imaging and spectroscopy show enhanced collective optical properties over the individual chromophores (ZnTPyP), favorable for exciton formation and transport.

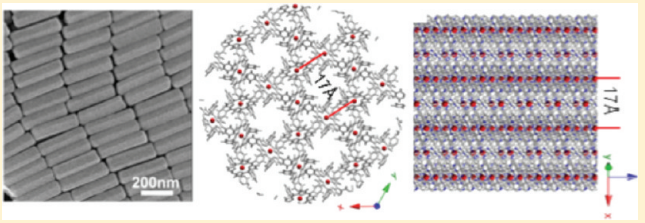

KEYWORDS: Hierarchical nanostructure, nanoporous, self-assembly, one-dimensional nanowire and nanorod, j-aggregate, porphyrin

Porous one-dimensional (1D) nanostructures, such as nanowires and nanorods, are materials of great interest for catalysis, sensing, and nanoelectronics due to their high surface areas and low densities.[1−3] Functionality of these nanomaterials is greatly expanded by incorporation of dye compounds, especially through J-aggregation of dye molecules that leads to strong excitonic coupling.[4] Continuous extensive efforts have been made to develop methods to fabricate 1D porous nanostructures,[1] such as templating methods,[5,6] hydrothermal synthesis,[7] noncovalent self-assembly,[8,9] and coordination modulation growth.[10] Despite these efforts, it is challenging to integrate multifunction into 1D nanostructures at multiple length scales and locations. Molecular self-assembly is one of the powerful methods to fabricate porous hierarchical nanostructures that impart multifunctionality derived from individual starting molecules or molecular building blocks.[3] Pore structures, morphologies, and function can be readily controlled by cooperative self-assembly through specific noncovalent interactions as well as variation of shape and size of starting molecules or building blocks. Harnessing these advantages, we report here a cooperative self-assembly process to synthesize highly ordered networks of 1D nanostructures that exhibit hierarchical structure and enhanced optical activity.

Porphyrins and related compounds, such as chlorophyll and heme, are essential to many biological energy transduction processes including light harvesting and photocatalytic processes.[11−13] Inspired by their utility and function, here we use their relative zinc meso-tetra (4-pyridyl) porphyrin (ZnTPyP) as our molecular building block. Whereas most porphyrins form H-aggregates as they typically self-assemble in a face-to-face manner via π-overlap,[14] ZnTPyP can self-assemble into more favorable arrangements via coordination of its peripheral pyridine groups to its core metal ions. ZnTPyP has well-defined size (~1.6 nm × 1.6 nm × 0.5 nm) and surface chemistry and is highly stable.

The first step in our confined self-assembly synthesis is encapsulation of ZnTPyP within the core of surfactant micelles through an interfacially driven aqueous process.[15] ZnTPyP does not readily dissolve in water, so it is acidified such that its pyridyl

Received: July 18, 2011
Revised: November 7, 2011
Published: November 15, 2011

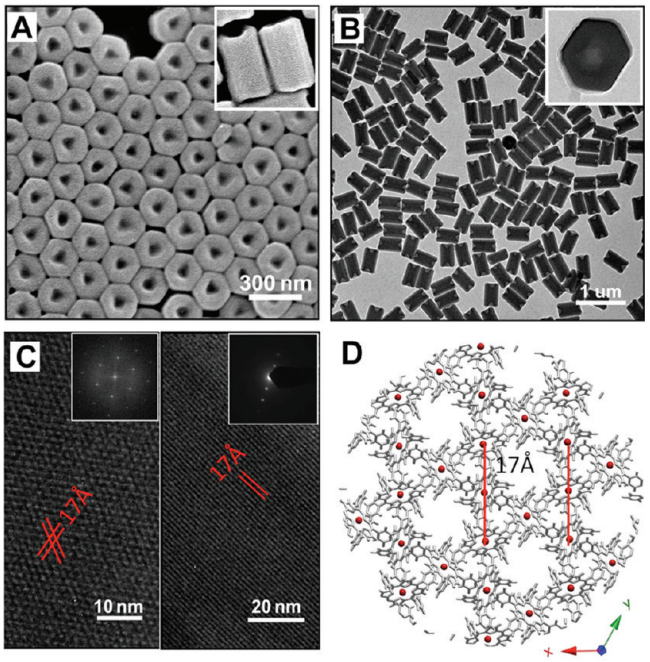

Figure 1. Structure of the self-assembled ZnTPyP nanostructures. (A) SEM images of monodisperse hexagonal rods prepared using 0.5 mM ZnTPyP (in 0.01 M HCl solution) and 0.01 M sodium dodecyl sulfate (SDS) at pH 11.3. Inset: cross-sectional SEM image of the nanorods. (B) Corresponding TEM image of the nanorods; inset: end view of a nanorod. (C) HR-TEM of the nanorods. Left: side view along the nanorod, inset shows the selected-area electron diffraction (SAED). Right: top view of the nanorod, inset shows the FFT. More HR-TEM images are provided in Supporting Information Figure S1. (D) Simulated crystal structure of hexagonal nanorods (plan-view), Zn (red) and C (gray).

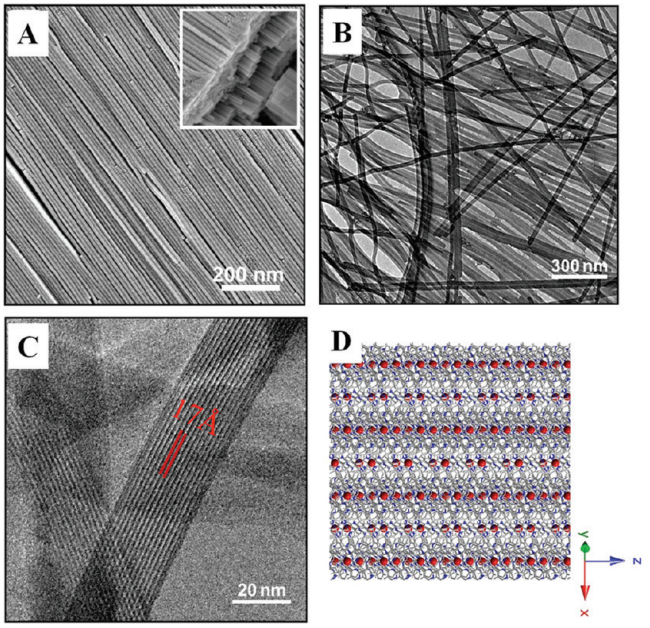

Figure 2. Structure of the self-assembled ZnTPyP nanostructures. (A) SEM image of the nanowires prepared using 0.5 mM ZnTPyP and 0.01 M cetyl trimethylammonium bromide (CTAB) at pH 9.5. (B) Corresponding TEM image of the nanowires. (C). HR-TEM image of the nanowires. (D). Simulated crystal structure of the nanowires viewed along the wire along the crystallographic *c*-axis, Zn (red), N (blue), and C (gray).

groups will be protonated and the resulting soluble tetrapyridinium cation ZnTPyP-H_4^{4+} forms a homogeneous solution.[16] The encapsulation process is initiated by adding this ZnTPyP-H_4^{4+} acidic aqueous solution to a basic aqueous solution of surfactant [$c_{surfactant}$ > critical micelle concentration (cmc)] under vigorous stirring with a range of volume ratios (see experimental details in Supporting Information). Acid−base neutralization deprotonates the tetrapyridinium cations, producing insoluble ZnTPyPs that are thus encapsulated within the hydrophobic micellar interiors as typically happens with hydrophobic nanoparticles or oil-like species.[15,17] Further self-assembly driven by intermolecular axial coordination (Zn−N) or noncovalent interactions such as hydrophobic−hydrophobic interactions and aromatic $\pi-\pi$ stacking between molecules or surfactants initiates nucleation and growth of J-aggregate ZnTPyP nanostructures.

The nanostructures produced have well-defined 1D morphologies, including nanorods and nanowires as illustrated in Figure 1. Figure 1A shows a representative scanning electron microscopy (SEM) image of the ZnTPyP nanorods, which have hexagonal external profile with narrow size distribution in both length and diameter. The average diameter of the nanorods is 150 nm (standard deviation 10%) and the aspect ratio can be controlled in a range from 2 to 10. The monodispersity of these nanorods allows them to further form ordered hexagonal arrays. Transmission electron microscopy (TEM) characterization (Figure 1B) reveals a uniform electron contrast in these 1D nanostructures, without defects. The cross-sectional TEM image (Figure 1B, inset) confirms that the nanorods exhibit hexagonal shape. High-resolution TEM (HR-TEM) (Figure 1C and Supporting Information Figure S1) demonstrates ordered pore arrays within a single crystalline wall structure. The plan view along the rod *c*-axis (Figure 1C, right) shows the hexagonal arrangement of the micropores; the pore diameter is measured to be 0.8 nm and the center-to-center distance 1.7 nm. The complementary side-view (Figure 1C, left) indicates that the pore channels run straight across the nanorod length, parallel to the outer surface profile. The periodicity is measured to be 1.7 nm, consistent with [110] orientation of hexagonal pore structures. Selected-area electron diffraction (SAED) of a single nanorod (Figure 1C, left inset) and fast Fourier transform (FFT) analysis (Figure 1C, right inset) show a single-crystalline pattern. Figure 2A shows SEM images for typical nanowires. The length of the nanowires can be controlled from ~1.5 to 6 μm. TEM imaging shows uniform electron contrast along the nanowires (Figure 2B). The diameter of the nanowires ranges from a few nanometers to tens of nanometers. HR-TEM (Figure 2C) indicates an ordered crystalline structure (pore channels) parallel to the nanowire surface profile. The periodicity is measured to be ~1.7 nm suggesting a similar crystal structure to that of the nanorods.

The crystal structures were further characterized by X-ray diffraction (XRD). XRD data show single crystal patterns with major peaks between 5 and 30° (see Supporting Information Figure S2). All of the peaks can be indexed as hexagonal space group $R\bar{3}$ with the unit cell dimensions $a = b = 33.110$ Å, $c = 9.273$ Å, $\alpha = \beta = 90°$, and $\gamma = 120°$.[18] Note that despite their different macroscopic morphologies (nanorod or nanowire), the 1D nanostructures exhibit the same XRD patterns indicating identical crystal structure and unit cell for the various morphologies. Figures 1D and 2D show the crystal structures simulated from

dx.doi.org/10.1021/nl203598n |*Nano Lett.* 2011, 11, 5196–5200

Table 1. Porosity, Surface Area, and Pore Size of Different ZnTPyP Nanostructures

	porosity (%)	surface area (m^2/g)	pore size (Å)
thin nanorods	34.3	371	8.1
hexagonal nanorods	20.1	327	7.9
nanowires	16.1	294	7.8

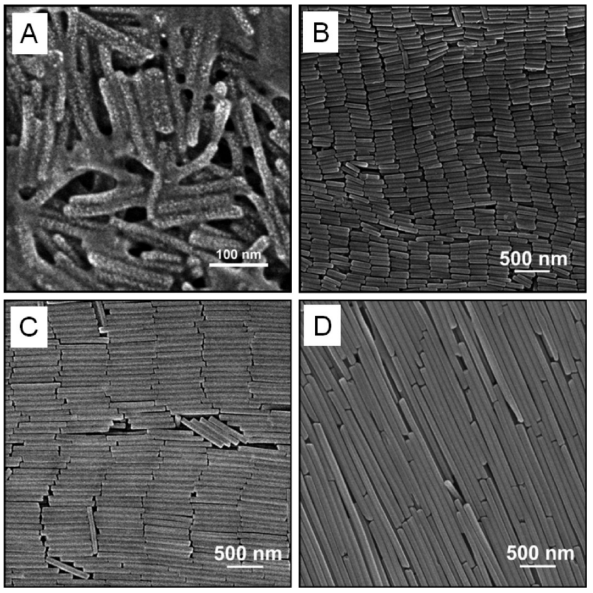

Figure 3. Representative SEM images showing controlled size and aspect ratio of 1D nanostructures. (A) diameter (d) = 15 nm, length (l) = 120 nm. (B) d = 35 nm, l = 280 nm. (C) d = 75 nm, l = 800 nm. (D) d = 100 nm, l = 2.5 μm.

the XRD data. In this structural model, each ZnTPyP molecule's central zinc atom is coordinated to two pyridyl N-atoms of neighboring ZnTPyPs approaching from both faces. In the framework, each ZnTPyP molecule is bound to four neighbors through four identical Zn−N axial ligations: two at its Zn core and two at opposite ends of its peripheral pyridyl groups, forming hexagonal shape micropores. This leaves two remaining pyridyl groups of ZnTPyP unligated and exposed at pore surfaces.

The adjacent circular hexametric cage arrays interpenetrate each other in the crystal structure through noncovalent $\pi-\pi$ interactions between ZnTPyP monomers, forming pore channels along the c-axis, parallel to the wall of the 1D nanostructures. On the basis of this model, the calculated pore size is 0.92 nm and the periodicity is 1.7 nm, consistent with TEM observations and values calculated from nitrogen isotherms (see Table 1). The confined cooperative self-assembly growth process advantageously allows control over size and aspect ratio of the 1D nanostructures that is not attainable by other methods.[2,4,9] Figure 3 shows typical SEM images of the 1D nanostructures with varied diameters and lengths.

The nanostructures exhibit remarkable optical properties that are quite different from the ZnTPyP monomers. Figure 4A shows the absorption spectra of the ZnTPyP nanorods and monomers. The intense Soret band (B-band) of the ZnTPyP monomer (at ~424 nm) becomes split upon self-assembly with a red-shifted band arising (at ~462 nm), indicative of J-aggregation. Although individually narrow, all combined the new bands cover a broader region of the spectrum. The Q-bands of the J-aggregate (~572

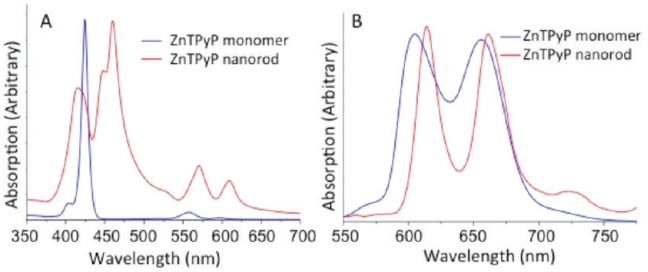

Figure 4. UV−vis absorption (A) and fluorescence spectra (B) of ZnTPyP monomers (blue) and nanorods (red).

and 611 nm) are hugely enhanced in intensity over their monomeric counterparts (at 557 and 597 nm). This is beneficial since it is the exciton coupling (proportional to the oscillator strength) between these states that is relevant for exciton transport.[19] The fluorescence image of the 1D nanowires is shown in Supporting Information Figure S3, and photoluminescence measurements of the nanorods reveal two emissions centered at ~613 and 660 nm that are narrower than their monomeric counterparts (Figure 4B). The nanorods exhibit a smaller Stokes shift than monomeric ZnTPyP, as is typical of J-aggregates.

Greater insight into the nanostructure growth process was gained by monitoring the time progression of the reaction under standard conditions by UV−vis spectroscopy and SEM (Figure 5). SDS surfactant system was used for the studies of the nanostructure growth mechnism. For reaction times below 4.5 h, SEM imaging shows no apparent nanostructures were formed. The Soret bands in the corresponding UV−vis spectra of ZnTPyP indicate only aggregated oligomers are formed. After 4.5 h, well-defined nanocrystals with hexagonal shape can be observed from SEM imaging. In SDS case, both the diameter and the length of the nanostructures increase with reaction time. SDS has negatively charged hydrophilic head groups that attract the tetrapyridinium cation ZnTPyP-H_4^{4+} to surround the SDS micelle surface. Once the acid−base neutralization occurs, a large quantity of neutral ZnTPyP monomers will be available for crystal growth, which leads to fast local growth kinetics. On the contrary, in the case of CTAB the positive micelle interface repels the tetrapyridinium cation ZnTPyP-H_4^{4+}. In such case, small seed crystals are formed preferably after the acid−base neutralization. Because of the lack of ZnTPyP monomers surrounding the micelles, further growth of the nanostructures is limited. Instead, self-assembly between small seeds into long wires is dominant.

Nitrogen sorption isotherms were measured to characterize the pore structures of the 1D nanostructures. Nitrogen adsorption/desorption isotherms and corresponding micropore size distributions for different 1D ZnTPyP nanostructures are shown in Figure 6. The calculated porosity, surface area, and average micropore size are summarized in Table 1. The nitrogen isotherms are characteristic of type I isotherms without apparent hysteresis. BET measurement shows a maximum surface area of 371 m^2/g for the nanorod structure. The pore size distribution shows a major peak at ~0.8 nm that corresponds to the hexagonal crystal lattice of self-assembled nanocrystals (Figure 1C). The porosity of these materials is maintained after degassing at 50 °C for 48 h suggesting stability of the pore structure. In addition to the micropore, there also exist mesopores and macropores ranging from 2 to 100 nm (Figure 6B) that is probably due to the packing of nanorods and nanowires.

dx.doi.org/10.1021/nl203598n |*Nano Lett.* 2011, 11, 5196–5200

Our thermogravimetric analysis (TGA) results recorded under argon atmosphere show that these materials are thermally stable up to ~450 °C before they are carbonized. In addition to physical sorption, we have discovered that these 1D nanostructures show a specific chemical sorption of NO. The nanorods show ~4 wt % NO absorption at 1 atm and ~34 wt % NO absorption at 10 atm (see Supporting Information Figure S4). We performed TGA on the specimens after exposure to NO to further confirm NO absorption. The results show a consistent weight loss at about ~190 °C (see Supporting Information Figure S5). Fourier transform infrared spectroscopy results suggest that NO coordinates to central Zn ions (see Supporting Information Figure S6).[20]

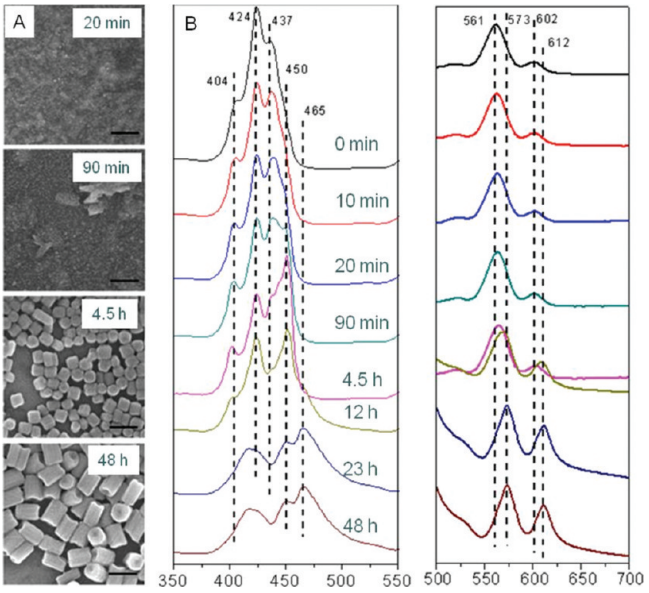

Figure 5. Time progression of ZnTPyP monomer aggregation to form nanostructures, monitored by (A) SEM imaging and (B) UV−vis absorption spectroscopy. In this reaction, 5 mL of stock ZnTPyP solution in water (0.01 M, 0.2 M HCl) was added into 95 mL of SDS 0.01 M solution (0.02 M NaOH) while stirring continuously at room temperature for 48 h. The 0.5 mL samples of the reaction mixture were withdrawn at different times for UV−vis spectra. The ZnTPyP nanostructures were separated for SEM imaging by centrifugation at 9000 rpm. The spectra here represent a superposition of the monomeric ZnTPyP molecules found in micellar interiors and their solubilized counterparts.[16]

It is worth noting that the position of the pyridyl groups' nitrogens relative to the macrocyclic ring and the choice of center metal ion are critical to the formation of well-defined morphology. Having the pyridyl nitrogen at the 4-position allows open space to coordinate with central Zn to form stable hexamers that direct further growth with increasing diameters and length. Our experiments indicated that 4-pyridyl monomers and Zn central metal are essential for the formation of 1D nanocrystals. By using 2-pyridyl substituents, 3-pyridyl substituents, or other core metal, we obtained 2D nanosheets and nanospheres instead of 1D nanostructures (see Supporting Information Figure S7). Detailed experiments also indicated that the presence of surfactants with concentration $C_{surfactant}$ higher than the cmc in the self-assembly system is essential. It was discovered that irregular structures were obtained in the absence of surfactants or for $C_{surfactant}$ lower than cmc (see Supporting Information Figure S8). Furthermore, we find that for single-tailed surfactants, an alkane chain of ten or more carbons is required to form well-defined crystalline nanostructures. This is similar to previous observations that concluded that surfactants with longer alkane chains are necessary for encapsulation of nanoparticles within surfactant micelles because longer alkane chains form more stable micelles to confine nucleation and growth of well-defined nanocrystals.[15] In experiments using ethanol as solvent instead of water, ill-defined nanostructures are obtained. This is probably because surfactants do not form micelles in ethanol and thus are not able to stabilize or confine the molecular assembly of macrocyclic monomers.

In summary, we have developed a facile confined cooperative self-assembly process to synthesize nanoporous 1D J-aggregate nanostructures. Through surfactant-assisted noncovalent interactions, nanorods and nanowires with controlled dimension and morphology can be prepared. The materials exhibit unique optical properties, enhanced over properties of individual monomers due to collective behavior resulting from their aggregation. Through kinetic control, our method readily allows for fine-tuning of nanostructure, dimension, and function on multiple length scales. At the molecular level, ZnTPyPs with well-defined size and chemistry possess unique optical and photocatalytic properties for potential synthesis of metallic structures. On the nanoscale, controlled assembly of macrocyclic monomers leads to formation of ordered nanostructures with precisely defined

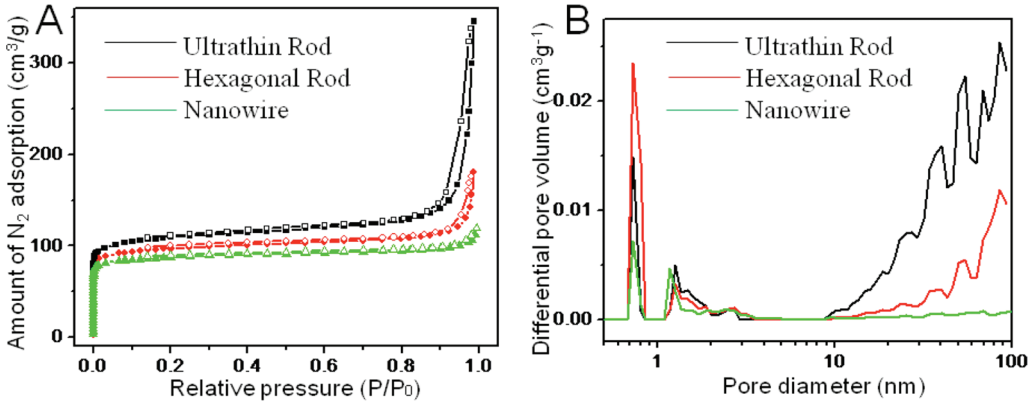

Figure 6. (A) Nitrogen sorption isotherms obtained at 77 K for different ZnTPyP nanostructures: ultrathin rods (diameter 15 nm, length 70 nm), hexagonal rods (diameter 120 nm, length 500 nm), and nanowires (diameter 100 nm, length 2.5 μm) (adsorption, solid data markers; desorption, open data markers). (B) Micropore size distributions for different ZnTPyP nanostructures.

dx.doi.org/10.1021/nl203598n |*Nano Lett.* 2011, 11, 5196–5200

size, shape, and spatial monomer arrangement so as to facilitate intermolecular mass and energy transfer or delocalization. The capability of exerting rational control over dimension and morphology provides new opportunities for applications in sensing,[21] nanoelectronics,[22] and optics.[23,24]

■ ASSOCIATED CONTENT

Supporting Information. Detailed experimental information, TEM, spectra, and XRD results are provided. This material is available free of charge via the Internet at http://pubs.acs.org.

■ AUTHOR INFORMATION

Corresponding Author
*E-mail: hfan@sandia.gov.

■ ACKNOWLEDGMENT

We thank Dr. Dongmei Ye for her valuable discussions and help on the paper. This work is supported by the U.S. Department of Energy, Office of Basic Energy Sciences, Division of Materials Sciences and Engineering, Sandia National Laboratories' LDRD program, National Science Foundation (DMI-0625897), and the National Natural Science Foundation of China (No. 21171049 and No. 50828302). TEM studies were performed in the Department of Earth and Planetary Sciences at University of New Mexico. We acknowledge the use of the SEM facility supported by the NSF EPSCOR and NNIN grants. Sandia is a multiprogram laboratory operated by Sandia Corporation, a wholly owned subsidiary of Lockheed Martin Corporation, for the U.S. Department of Energy's National Nuclear Security Administration under Contract DE-AC04-94AL85000.

■ REFERENCES

(1) Zang, L.; Che, Y.; Moore, J. S. *Acc. Chem. Res.* **2008**, *41* (12), 1596–1608.
(2) Wang, Z.; Medforth, C. J.; Shelnutt, J. A. *J. Am. Chem. Soc.* **2004**, *126* (49), 15954–15955.
(3) Stupp, S. I.; LeBonheur, V.; Walker, K.; Li, L. S.; Huggins, K. E.; Keser, M.; Amstutz, A. *Science* **1997**, *276* (5311), 384–389.
(4) Würthner, F.; Kaiser, T. E.; Saha-Möller, C. R. *Angew. Chem., Int. Ed.* **2011**, *50* (15), 3376–3410.
(5) Li, F.; He, J.; Zhou, W. L.; Wiley, J. B. *J. Am. Chem. Soc.* **2003**, *125* (52), 16166–16167.
(6) Gan, H.; Liu, H.; Li, Y.; Liu, Y.; Lu, F.; Jiu, T.; Zhu, D. *Chem. Phys. Lett.* **2004**, *399* (1−3), 130–134.
(7) Wang, P.-p.; Bai, B.; Hu, S.; Zhuang, J.; Wang, X. *J. Am. Chem. Soc.* **2009**, *131* (46), 16953–16960.
(8) Wang, Z.; Medforth, C. J.; Shelnutt, J. A. *J. Am. Chem. Soc.* **2004**, *126* (51), 16720–16721.
(9) Hu, J.-S.; Guo; Liang, H.-P.; Wan, L.-J.; Jiang, L. *J. Am. Chem. Soc.* **2005**, *127* (48), 17090–17095.
(10) Tsuruoka, T.; Furukawa, S.; Takashima, Y.; Yoshida, K.; Isoda, S.; Kitagawa, S. *Angew. Chem., Int. Ed.* **2009**, *48* (26), 4739–4743.
(11) Mauzerall, D. C. *Clin. Dermatol.* **1998**, *16* (2), 195–201.
(12) Drain, C. M.; Varotto, A.; Radivojevic, I. *Chem. Rev.* **2009**, *109* (5), 1630–1658.
(13) Blankenship, R. E. *Molecular Mechanisms of Photosynthesis*: Blackwell: Oxford, 2002.
(14) Eisfeld, A.; Briggs, J. S. *Chem. Phys.* **2006**, *324* (2−3), 376–384.
(15) Fan, H.; Yang, K.; Boye, D. M.; Sigmon, T.; Malloy, K. J.; Xu, H.; Lopez, G. P.; Brinker, C. J. *Science* **2004**, *304* (5670), 567–571.
(16) Bai, F.; Wu, H.; Haddad, R. E.; Sun, Z.; Schmitt, S. K.; Skocypec, V. R.; Fan, H. *Chem. Commun.* **2010**, *46* (27), 4941–4943.
(17) Barber, D. C.; Freitag-Beeston, R. A.; Whitten, D. G. *J. Phys. Chem.* **2002**, *95* (10), 4074–4086.
(18) Krupitsky, H.; Stein, Z.; Goldberg, I.; Strouse, C. E. *J. Inclusion Phenom.* **1994**, *18*, 177.
(19) Siebbeles, L. D. A.; Grozema, F. *Charge and Exciton Transport through Molecular Wires*: Wiley-VCH: New York, 2011.
(20) Israelachvili, J. N.; Mitchell, D. J.; Ninham, B. W. *J. Chem. Soc.* **1976**, *2*, 1525–1568.
(21) Rakow, N. A.; Suslick, K. S. *Nature* **2000**, *406*, 710–713.
(22) Schwab, A. D.; Smith, D. E.; Bond-Watts, B.; Johnston, D. E.; Hone, J.; Johnson, A. T.; de Paula, J. C.; Smith, W. F. *Nano Lett.* **2004**, *4* (7), 1261–1265.
(23) Winkelmann, C. B.; Ionica, I.; Chevalier, X.; Royal, G.; Bucher, C.; Bouchiat, V. *Nano Lett.* **2007**, *7* (6), 1454–1458.
(24) Medforth, C. J.; Wang, Z.; Martin, K. E.; Song, Y.; Jacobsen, J. L.; Shelnutt, J. A. *Chem. Commun.* **2009**, *46* (47), 7261–7277.